Intercarrier Interference Immune Single Carrier OFDM via Magnitude-Keyed Modulation for High Speed Aerial Vehicle Communication

Xue Li, *Student Member, IEEE,* Steven Hong, *Student Member, IEEE,* Vasu D. Chakravarthy, *Member, IEEE,* Michael Temple, *Senior Member, IEEE,* and Zhiqiang Wu, *Member, IEEE*

***Abstract*—Orthogonal Frequency Division Multiplexing (OFDM) has been considered as a strong candidate for next generation wireless communication systems. Compared to traditional OFDM, Single Carrier OFDM (SC-OFDM) has demonstrated excellent bit error rate (BER) performance, as well as low peak to average power ratio (PAPR). Similar to other multi-carrier transmission technologies, SC-OFDM suffers significant performance degradation resulting from intercarrier interference (ICI) in high mobility environments. Existing techniques for OFDM can be directly adopted in SC-OFDM to improve performance, however, this improved performance comes at costs such as decreased throughput. In this paper, we analyze the effect of ICI on an SC-OFDM system and propose a novel modulation scheme. The proposed Magnitude-Keyed Modulation (MKM) modulation provides SC-OFDM system immunity to ICI and with an easy implementation it significantly outperforms OFDM, SC-OFDM and MC-CDMA systems with Phase Shift Keying (PSK) modulation and Quadrature Amplitude Modulation (QAM) in severe ICI environment. Analysis also illustrates the proposed SC-OFDM system with MKM modulation maintains low PAPR compared to traditional OFDM and SC-OFDM systems with PSK and QAM modulations. Simulation results for different modulation schemes in various ICI environments confirm the effectiveness of the proposed system.**

***Index Terms*—**

I. Introduction

ORTHOGONAL Frequency Division Multiplexing (OFDM) and other multi-carrier transmission technologies such as Multi-Carrier Code Division Multiple Access (MC-CDMA) have been considered strong candidates for next generation high-data-rate wireless communication systems because of their good BER performance and high spectrum efficiency [1]. It is highly desired to adopt multi-carrier transmission in aerial vehicle communication to improve the spectrum efficiency.

In multi-carrier transmission technology such as OFDM, it is crucial to maintain orthogonality among all the subcarriers. Otherwise, intercarrier interference (ICI) will occur and lead to significant performance degradation. In a high mobility environment such as aerial vehicle communication, multi-carrier transmission technologies experience severe ICI due to Doppler shift introduced by high mobility of transmitter or receiver, or both. Many studies have been conducted in evaluating the BER performance of OFDM system and MC-CMDA system with ICI [2], [3] and improving the performance by reducing ICI for OFDM [4]–[10] or by estimating the carrier frequency offset (CFO) [11]–[13]. Such techniques are effective in low mobility environments where the speed variation is low. For example, training symbols can be transmitted in the packet header for *multiple* OFDM symbols to aid the receiver in obtaining the CFO estimate. If the relative transmitter–receiver speed is not changing during packet transmission, the overhead of sending such training symbols is negligible. However, in aerial vehicle communication, the relative transmitter–receiver speed changes so rapidly that it is unreasonable to assume a constant speed (and CFO) during the entire packet transmission. Hence, to accurately estimate the CFO, training symbols need to be transmitted for *every* OFDM symbol. Obviously, this significantly reduces OFDM throughput while adding complexity due to repeated CFO estimation.

On the other hand, the Single Carrier Orthogonal Frequency Division Multiplexing (SC-OFDM) [14] technique has received a lot of attention as an alternative transmission technique to the conventional OFDM due to its better performance in multipath fading channels and lower peak to average power ratio (PAPR). SC-OFDM and similar technologies have been independently developed by multiple research groups almost simultaneously. For example, Single Carrier Frequency Domain Equalization (SCFDE) [15]–[18] and Carrier Interferometry Orthogonal Frequency Division Multiplexing (CI/OFDM) [19]–[21] are essentially the same technology. They combine benefits of multi-carrier transmission with single carrier

Paper approved by H. Leib, the Editor for Communication and Information Theory of the IEEE Communications Society. Manuscript received March 19, 2011; revised August 18, 2012.

This paper was presented in part at the *IEEE GLOBECOM* conference, Honolulu, Hawaii, USA, 2009, and demonstrated in part at *IEEE GlobeCOM* conference, Miami, Florida, USA, 2010, and received the Best Demo Award.

This work is supported in part by National Science Foundation under Grants No. 0708469, No. 0737297, No. 0837677, the Wright Center for Sensor System Engineering, and the Air Force Research Laboratory.

X. Li is with the Department of Electrical Engineering, Wright State University, Dayton, OH, USA. Steven Hong is with the Department of Electrical Engineering, Stanford University, Stanford, CA, USA (e-mail: hsiying@stanford.edu).

V. D. Chakravarthy is with the Air Force Research Laboratory, Wright-Patterson AFB, OH, USA (e-mail: vasu.chakravarthy@wpafb.af.mil).

M. Temple is with Department of Electrical and Computer Engineering, Air Force Institute of Technology, Dayton, OH, USA (e-mail: michael.temple@afit.edu).

Z. Wu is with the Department of Electrical Engineering, Wright State University, Dayton, OH, USA (e-mail: zhiqiang.wu@wright.edu).

Digital Object Identifier 10.1109/TCOMM.2012.09.110214

transmission using a cyclic prefix to allow frequency domain processing at receiver to exploit frequency diversity.

In this paper, we analyze SC-OFDM system with ICI and show a unique diagonal property of SC-OFDM with ICI. Due to this property, the ICI effect on SC-OFDM is concentrated entirely on the phase offset and not on the magnitude. We then propose a novel modulation scheme called Magnitude-Keyed Modulation (MKM) for SC-OFDM. As the name suggests, this new modulation scheme carries digital data only on the signal magnitude. Hence, MKM provides SC-OFDM with immunity to ICI, i.e., the BER performance of a SC-OFDM system with MKM does not depend on the ICI. Given the MKM is a non-coherent modulation scheme, the proposed SC-OFDM with MKM modulation performs slightly worse than SC-OFDM (or OFDM or MC-CDMA) with PSK (or QAM) modulation when there is no ICI. However, the performance of SC-OFDM (or OFDM or MC-CDMA) with PSK (or QAM) modulation has obvious degradation in severe ICI environment or with high modulation schemes, and the new system significantly outperforms them. Compared with existing ICI cancellation schemes or CFO estimation schemes, the proposed modulation technique does not need to sacrifice the data rate via employing training sequence or self-cancellation coding, meanwhile it is totally immune to the ICI. Additionally, the proposed system has low complexity and is easy to be implemented. Meanwhile, the lower PAPR property of SC-OFDM system is also maintained for the proposed system. Hence, the proposed SC-OFDM system is an ideal candidate for high speed aerial vehicle communication. Simulation results for different levels of modulation schemes in different ICI environments confirm the effectiveness of the proposed system.

The rest of the paper is organized as follows: In Section II, we present the OFDM and SC-OFDM system models. Literature reviews of some existing ICI cancellation and CFO estimation schemes are provided in Section III. Section IV presents the analysis of ICI and demonstrates an important diagonal property of ICI matrix in SC-OFDM. We then propose MKM modulation for SC-OFDM which is immune to ICI and also analyze the theoretical BER performance and PAPR performance in Section V. Section VI shows the simulation results which confirm our analysis, and conclusion is given in Section VII.

II. System Model

A. OFDM System

In the OFDM transmitter, after a constellation mapping for the appropriate modulation, (QAM, PSK, etc.), data symbols are converted from serial to parallel. Assuming there are N subcarriers in the OFDM system, each OFDM block contains a set of N symbols $(x_0, x_1, ..., x_{N-1})$, assigned to N subcarriers using an N-point IFFT.

Accounting for all N symbols, the composite complex OFDM signal is given by

$$s(t) = \sum_{k=0}^{N-1} x_k e^{j2\pi k\Delta f t} e^{j2\pi f_c t} p(t) \tag{1}$$

where x_k is the k^{th} data symbol; Δf is the spacing between subcarriers; and $p(t)$ is a rectangular pulse shape with time limit spanning one OFDM symbol, $0 \le t \le T$. To ensure orthogonality among subcarriers, we have $\Delta f = 1/T = 1/NT_b$ where T_b is the data symbol period.

Following transmission, channel propagation, and cyclic prefix removal, the signal at the receiver corresponds to

$$r(t) = \sum_{k=0}^{N-1} \alpha_k x_k e^{j2\pi(k\Delta f + f_0)(t+\Delta t)} e^{j2\pi f_c(t+\Delta t)} p(t+\Delta t) + n(t) \ , \tag{2}$$

where $n(t)$ is additive white Gaussian noise (AWGN), α_k is the complex fading gain on the k^{th} subcarrier, Δt represents the time delay and f_0 is the CFO. Here we denote the normalized carrier frequency offset (NCFO) as $\varepsilon = f_0/\Delta f$ and rewrite the received OFDM signal as

$$r(t) = \sum_{k=0}^{N-1} \alpha_k x_k e^{j2\pi(k+\varepsilon)\Delta f(t+\Delta t)} e^{j2\pi f_c(t+\Delta t)} p(t+\Delta t) + n(t) \ . \tag{3}$$

The OFDM demodulator detects each symbol by decomposing $r(t)$ in (3) onto N orthogonal subcarriers (via application of an FFT), where perfect timing estimation is assumed. If the NCFO is zero, the received signal on the k^{th} subcarrier simply equals to $y_k = x_k\alpha_k + n_k$. However, when the NCFO is non-zero, the received signal on the k^{th} subcarrier corresponds to

$$y_k = x_k\alpha_k S(0) + \sum_{l=0, l\neq k}^{N-1} x_l\alpha_l S(l-k) + n_k, \qquad k = 0, 1, \ldots, N-1 \ , \tag{4}$$

where the first term is the *desired* signal component $y_k^d = x_k\alpha_k S(0)$, the second term is the *ICI* component

$$y_k^{ICI} = \sum_{l=0, l\neq k}^{N-1} x_l\alpha_l S(l-k) \ , \tag{5}$$

and $S(l-k)$ is the ICI coefficient from l^{th} subcarrier to k^{th} subcarrier:

$$S(l-k) = \frac{\sin\left[\pi(\varepsilon + l - k)\right]}{N\sin\left[\frac{\pi}{N}(\varepsilon + l - k)\right]} \cdot \exp\left[j\pi\left(1 - \frac{1}{N}\right)(\varepsilon + l - k)\right] \ . \tag{6}$$

Now denoting $\vec{x} = \{x_0, x_1, \ldots, x_{N-1}\}$ as the transmitted symbol vector, $\vec{y} = \{y_0, y_1, \ldots, y_{N-1}\}$ as the received signal vector, $\vec{n} = \{n_0, n_1, \ldots, n_{N-1}\}$ as the noise vector, and $\mathbf{H} = diag\{\alpha_0, \alpha_1, \ldots, \alpha_{N-1}\}$ as the channel fading gain matrix, we have

$$\vec{y} = \vec{x}\mathbf{H}\mathbf{S} + \vec{n} \ , \tag{7}$$

where $\mathbf{S}$ is the ICI coefficient matrix having dimension $N \times N$ with p^{th}-row and q^{th}-column elements given by $\mathbf{S}_{p,q} = S(p-q)$. The resultant matrix form of $\mathbf{S}$ is:

$$\mathbf{S} = \begin{bmatrix} S(0) & S(-1) & \ldots & S(1-N) \\ S(1) & S(0) & \ldots & S(2-N) \\ \vdots & \vdots & \ddots & \vdots \\ S(N-1) & S(N-2) & \cdots & S(0) \end{bmatrix} \tag{8}$$

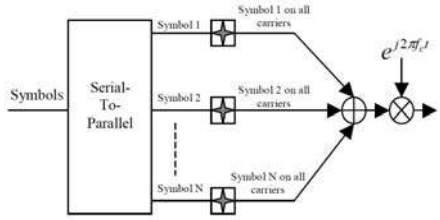

(a) SC-OFDM Spread Symbol Combining

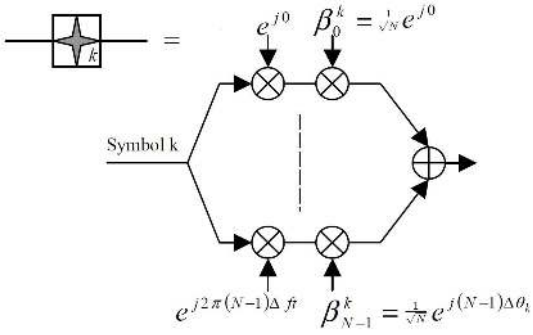

(b) SC-OFDM Symbol Spectral Spreading

Fig. 1. SC-OFDM Transmitter

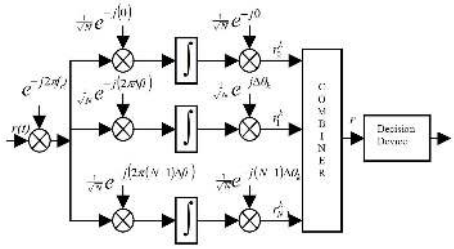

Fig. 2. SC-OFDM Receiver

B. Single Carrier OFDM System

Single Carrier OFDM (SC-OFDM) [14] and other similar technologies [15]- [21] combine benefits of multi-carrier transmission with single carrier transmission using a cyclic prefix and frequency domain processing.

Conceptual representations of the SC-OFDM transmitter and receiver are shown in Fig. 1 and Fig. 2 [20], respectively. Compared to a conventional OFDM system, the SC-OFDM system distributes each parallel data set to all sub-carriers using different phase-rotated spectral spreading on each symbol [14], as illustrated in Fig. 1(b). The spreading code set corresponds to the normalized DFT matrix with the k^{th} data symbol being spread to the i^{th} subcarrier employing spreading code $\beta_i^k = \frac{1}{\sqrt{N}} \exp(-j\frac{2\pi}{N}ik)$. Accounting for β_i^k and a block of N total data symbols, the transmitted SC-OFDM symbol corresponds to

$$s(t) = \frac{1}{\sqrt{N}} \sum_{i=0}^{N-1} \sum_{k=0}^{N-1} x_k e^{-j\frac{2\pi}{N}ik} e^{j2\pi i\Delta f t} e^{j2\pi f_c t} p(t) \ , \quad (9)$$

where variable definitions remain unchanged from (1).

The SC-OFDM system can be easily implemented using an MC-CDMA framework by making appropriate changes to the spreading code. Specifically, SC-OFDM system can be implemented as a fully loaded MC-CDMA system with new spreading code β_i^k, for example, transmitting N symbols using N subcarriers can be implemented as an MC-CDMA system with N users (each symbol can be viewed as an user in MC-CDMA system) using spreading code β_i^k. Hence, the SC-OFDM system uses the same bandwidth as the conventional OFDM or MC-CDMA system. Similar to an OFDM system, SC-OFDM can also be implemented using FFT and IFFT transforms.

The received SC-OFDM signal $r(t)$ for the transmitted signal in (9) is given by

$$r(t) = \frac{1}{\sqrt{N}} \sum_{i=0}^{N-1} \alpha_i \sum_{k=0}^{N-1} x_k e^{-j\frac{2\pi}{N}ik} e^{j2\pi(i+\varepsilon)\Delta f(t+\Delta t)} e^{j2\pi f_c(t+\Delta t)} \cdot p(t+\Delta t) + n(t) \ , \quad (10)$$

where variable definitions remain unchanged from (2).

At the SC-OFDM receiver shown in Fig. 2, the SC-OFDM demodulator detects the k^{th} data symbol by: 1) decomposing the received signal $r(t)$ into N orthogonal subcarriers (via application of an FFT, and perfect timing estimation is assumed), 2) applying the k^{th} symbol's spreading code, 3) combining the N results $\left\{r_0^k, r_1^k, ..., r_{N-1}^k\right\}$ with an appropriate combining scheme [22], denoted by the "Combiner" block in Fig. 2, 4) decision of each symbol will be made based on the result from the "Combiner", denoted by the block "Decision Device".

Similar to the OFDM system with ICI present and non-zero NCFO in (4), the received signal for the l^{th} SC-OFDM data symbol x_l corresponds to:

$$r_l = \frac{1}{N} \sum_{k=0}^{N-1} x_k S(k-l) \cdot \left[\sum_{i=0}^{N-1} w_i \alpha_i \exp\left(j\frac{2\pi}{N}l \cdot i\right) \exp\left(-j\frac{2\pi}{N}k \cdot i\right)\right] + n_l \quad (11)$$
$$\textit{where } l = 0, 1, ..., N-1$$

where w_i denotes the combining weight. By assuming Equal-Gain Combining (EGC) scheme has been applied [22], we have $w_i = 1$. It is clear that the l^{th} decoded data symbol r_l contains a *desired* signal component, given by (11) with $k = l$ as

$$r_l^d = \frac{1}{N} x_l S(0) \left[\sum_{i=0}^{N-1} \alpha_i \exp\left(j\frac{2\pi}{N}l \cdot i\right) \exp\left(-j\frac{2\pi}{N}l \cdot i\right)\right] = \frac{1}{N} x_l S(0) \sum_{i=0}^{N-1} \alpha_i \quad (12)$$

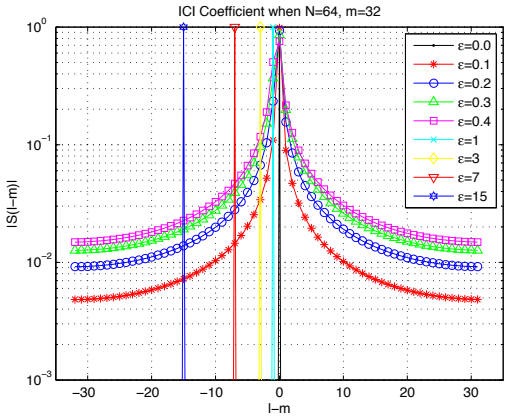

Fig. 3. Normalized ICI Coefficient Magnitude

and an *undesired* ICI component, given by (11) with $k \neq l$ as

$$r_l^{ICI} = \frac{1}{N} \sum_{k=0, k\neq l}^{N-1} x_k S(k-l) \cdot \left[\sum_{i=0}^{N-1} \alpha_i \exp\left(j\frac{2\pi}{N} l \cdot i\right) \exp\left(-j\frac{2\pi}{N} k \cdot i\right) \right] . \quad (13)$$

Using the vector and matrix notation introduced in (7), the received SC-OFDM signal vector is given by

$$\vec{r} = \vec{x}\mathbf{FHS} + \vec{n} \ , \quad (14)$$

where matrix $\mathbf{F}$ is the normalized DFT matrix acts to spread the SC-OFDM signal and is defined as

$$\mathbf{F}(n,k) = \frac{1}{\sqrt{N}} \exp\left(-j\frac{2\pi}{N} kn\right), \quad k,n \in [0, N-1] \ . \quad (15)$$

After applying EGC technique in the receiver, the combined signal vector becomes

$$\vec{y} = \vec{r}\mathbf{F}^H = \vec{x}\mathbf{FHSF}^H + \vec{n}\mathbf{F}^H \ , \quad (16)$$

where $\mathbf{F}^H$ is the conjugate transpose of matrix $\mathbf{F}$.

By comparing with the corresponding OFDM signal vector in (7), the SC-OFDM expression in (16) includes additional Fourier transform operations due to spreading codes being applied. These linear operations help simplify ICI analysis which is why we concentrate on ICI effects in SC-OFDM versus OFDM or MC-CDMA systems.

C. Intercarrier Interference

From the earlier definition of NCFO ($\varepsilon = f_0/\Delta f$), the NCFO can contain both integer and fractional components with each having different effects on the system. The ICI coefficient in (6) is periodic with period N, i.e., $S_{N+\varepsilon} = S_\varepsilon$, and has two responses associated with the integer and fractional values of ε. The magnitude of S, $|S(l,k)|$ in dB, is illustrated in Fig. 3 for various values of ε using $N = 64$ subcarriers.

In Fig. 3 for fractional ε variation, the dominant energy response of S converges to $S(0)$ when $\varepsilon = 0$. However, as ε varies fractionally from 0.1 to 0.4, the energy in S spreads across all subcarriers. For larger ε values there is a higher percentage of energy "leakage" across the subcarriers. However, it is important to note that dominant energy response of S remains in the $S(0)$ component. Hence, when ε is a fractional value: 1) $S(0)$ remains the largest component, 2) the largest weight in y_k of (4) will be x_k, and 3) the decision for $\hat{x}_k$ based on y_k remains reliable.

Fig. 3 also illustrates the ICI coefficient behavior for integer ε variation. From the definition, integer ε variation corresponds to a frequency offset whereby different subcarriers are identically mistaken. Hence, when $\varepsilon = l \ \ \{l \in \mathbb{Z}\}$: 1) $S(0)$ is not the largest component and the dominant response becomes the $S(l)$ component, 2) the largest weight in y_k of (4) will be x_{k+l}, and 3) the decision for $\hat{x}_k$ based on y_k will be unreliable with very high probability.

III. Existing ICI Reduction Techniques

Since CFO-dependent ICI can significantly degrade system performance due to coefficient energy leakage and dominant response shift as illustrated in Fig. 3, it is of great interest to study system performance in a mobile environment with ICI present. Many studies have been conducted to evaluate OFDM and MC-CMDA system BER with ICI present [2], [3] and several technologies have been developed to reduce ICI effects.

Taking advantage of ICI coefficient properties in Fig. 3, ICI self-cancellation technologies have been proposed and developed to cancel the fractional CFO component. A simple and effective ICI self-cancellation scheme has been proposed by Zhao and Haggman [4] who used polynomial coding in the frequency domain to mitigate the effect of fractional CFO. When compared to a coded system operating at a similar rate, their self-cancellation scheme provided better performance. In [7], an ICI self-cancellation scheme is adopted to combat the ICI caused by phase noise in OFDM systems. For more general cases, Seyedi and Saulnier proposed a general ICI self-cancellation scheme that can be implemented using windowing [5]. In [6], Ryu studied ICI self-cancellation using a data-conjugate method to effectively reduce ICI. However, these ICI self-cancellation schemes mitigate ICI at the cost of reduced data rate. This limitation was addressed in additional MC-CDMA work that considered a self-cancellation scheme that maintained the data rate [9].

In addition to self-cancellation techniques, other ICI cancellation schemes have been proposed. For example, work in [10] proposed an ICI cancellation scheme that does not lower transmission rate or reduce bandwidth efficiency. At the same time, the technique offers perfect ICI cancellation and significant BER improvement at linearly growing cost. Regardless of the ICI cancellation scheme, there is always an associated cost for improvement and trade-offs must be made, e.g., data rate and bandwidth efficiency may be maintained at the expense of greater implementation complexity, or, data rate and bandwidth efficiency may be sacrificed and less complex implementations employed. The importance of these trade-offs become even more important when considering cases where the CFO includes both integer and fractional components. In these cases, the ICI coefficient experiences both leakage and shift and the aforementioned cancellation schemes will require

even greater complexity to achieve similar performance with no guarantee of effectiveness.

Regardless of the components present in ε, it is readily apparent that if ε is known at the receiver the ICI can be totally canceled. Hence, researchers have spent considerable effort to improve ICI cancellation performance by estimating both the integer and fractional CFO components. Generally speaking, these existing CFO estimation schemes can be classified as either data aided or blind estimators. While data aided estimators [11]–[13] provide better estimation performance, they also reduce the effective data rate given that pilot data is transmitted. Hence, the blind estimators have received a lot of attention due to system power and high bandwidth efficiencies. The blind estimator in [23] utilizes an estimation algorithm based on maximum likelihood criteria and exploits the cyclic prefix preceding the OFDM symbols to estimate the CFO. As implied by its name, the Minimum Output Variance (MOV) estimator utilizes minimum output variance criteria to estimate CFO [24]. Work in [25] presents a non-data aided CFO estimator that utilizes criteria based on minimum received symbol power. Subsequent work in [26] and [27] estimate CFO by exploiting features in a smoothed power spectrum. The subspace method in [28] is based on channel correlation and the kurtosis CFO estimator in [29] is based on measuring non-Gaussian properties of the received signal. However, each of these existing blind CFO estimators have inherent drawbacks and efficient performance requires: 1) a constant modulus (CM) constellation, 2) a large number of OFDM blocks, and/or 3) knowledge of the channel order. In general, the performance of current blind estimators is not sufficient for high speed aerial vehicle communications. To address these drawbacks, we recently proposed a high accuracy blind CFO estimator for OFDM systems [30]. However, the data rate reduction and implementation complexity were both higher than what we expected, and the system performance will likely degrade given residual CFO is present in all estimation methods. To address this and other drawbacks of existing techniques, we analyze ICI coefficients in next section.

IV. ICI Coefficient Analysis

To provide an initial understanding how the ICI coefficient impacts system performance, we first focus our attention an AWGN channel. In this case, the channel gain fading matrix $\mathbf{H}$ becomes an identity matrix $\mathbf{I}$. For the analysis we must determine the ICI power. This can be done using the Carrier-to-Interference Power Ratio (CIR), defined as [4], [31]:

$$CIR = \frac{Desired\ Signal\ Power}{ICI\ Power}\ . \tag{17}$$

However, when there is no ICI present, e.g., $\varepsilon \to 0$, the CIR approaches infinity which cannot be shown in a figure. As an alternative approach, the ICI power can be estimated using the Interference-to-Carrier Power Ratio (ICR), defined as:

$$ICR = CIR^{-1} = \frac{ICI\ Power}{Desired\ Signal\ Power}\ . \tag{18}$$

The expression in (18) implies that the ICR becomes smaller as the desired signal power to ICI power ratio increases. It is evident that ICR is system dependent and thus critical for us to consider several possible cases. In our ICR simulations, we average the ICR across all subcarriers, which represents a more reliable approach relative to what was used in [4]. Specifically, ICR on k^{th} subcarrier can be represented as $ICR(k)$ = ICI power from non-k^{th} subcarrier / Signal power on k^{th} subcarrier. The average ICR, which is represented as $\frac{1}{N}\sum_{k=0}^{N-1} ICR(k)$, is compared in this paper; while $ICR(0)$ or $CIR(0)$ is compared in literature [4].

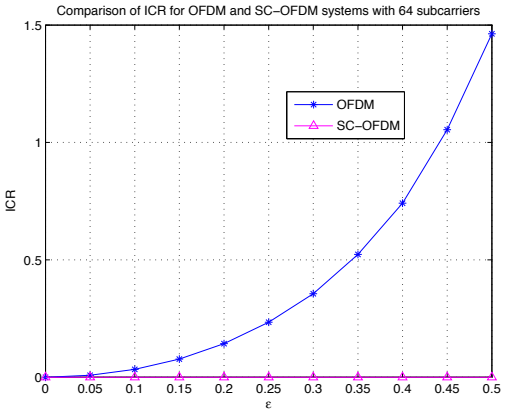

Fig. 4. ICR Comparison for OFDM and SC-OFDM Systems Using $N = 16$ Subcarriers with ICI Present.

Results in Fig. 4 show ICR versus ε for OFDM and SC-OFDM systems using $N = 16$ subcarriers over an AWGN channel with ICI present. It is evident that ICR of SC-OFDM is zero for all ε values, meaning the desired signal component used for data estimation is unaffected by ICI. Given the CIR of SC-OFDM is much lower than that of the OFDM system, the benefit of using SC-OFDM under conditions with ICI present are clearly evident by comparing to traditional OFDM under similar conditions. The following analysis of OFDM and SC-OFDM systems with ICI present is provided to show how ICI affects overall performance and helps explain why the SC-OFDM system experiences zero ICR.

A. Analysis of OFDM Performance with ICI Present

The received OFDM signal for an AWGN channel can be simply expressed using (7) with $\mathbf{H} = \mathbf{I}$ as

$$\vec{y} = \vec{x}\mathbf{S} + \vec{n}. \tag{19}$$

The received signal y_k for the k^{th} subcarrier is given by

$$y_k = \vec{x}\mathbf{S}(:,k) + n_k = x_k S(0) + \sum_{l=0, l\neq k}^{N-1} x_l S(l-k) + n_k \tag{20}$$

where $\mathbf{S}(:,k)$ is used to denote all elements in the k^{th} column of $\mathbf{S}$. Considering desired and undesired signal components separately, the corresponding power in the *desired* signal component $x_k S(0)$ is

$$E[\ |Desired\ Signal|^2\ ] = E\left[\ |x_k S(0)|^2\ \right]\ , \tag{21}$$

and the *undesired* ICI power is

$$E[\,|ICI|^2\,] = E\left[\left|\sum_{l=0,l\neq k}^{N-1} x_l S(l-k)\right|^2\right] , \quad (22)$$

which is clearly dependent on the combined symbol weights in $\vec{x}$, excluding x_k.

Taking the ratio of (22) to (21) per the definition in (18), the ICR for OFDM is given by

$$\begin{aligned} ICR_{OFDM} &= \frac{E[\,|ICI|^2\,]}{E[\,|Desired\ Signal|^2\,]} \\ &= \frac{E[\,|\sum_{l=0,l\neq k}^{N-1} x_l S(l-k)|^2\,]}{E[\,|x_k S(0)|^2\,]} \end{aligned} \quad (23)$$

Considering the limiting case when no ICI exists and $\varepsilon \to 0$, the ICI coefficient matrix in (19) becomes $\mathbf{S} = \mathbf{I}$ and the received signal vector simply reduces to the transmitted signal vector plus noise $\vec{y} = \vec{x} + \vec{n}$, thereby simplifying the detection decision. However, in cases with $\varepsilon \neq 0$ system performance degrades significantly. This occurs because CFO causes $\mathbf{S}$ in (19) to be non-diagonal which causes the target symbol's amplitude and phase to be weighted by $S(0)$, while at the same time mixing in non-target symbol contributions weighted according to $S(1-N), ..., S(-1)$ and $S(1), ..., S(N-1)$ in (8). Thus, to reliably determine $\vec{x}$, three unknowns are required: 1) target symbol amplitude change, 2) target symbol phase change, and 3) mixing weights of non-target symbols. To determine these unknowns, we can decompose $\mathbf{S}$ into separate related components and solve for them separately.

Using the received signal expression in (19), with a known ICI coefficient matrix $\mathbf{S}$ and $\mathbf{S}^{-1}$ existing, $\vec{x}$ can be reconstructed using $\vec{y}$. It is evident in (8) that the ICI coefficient matrix $\mathbf{S}$ is a circulant matrix which reduces the uncertainty of the $N \times N$ matrix from N^2 to $2N-1$. However, we know there is actually only one uncertainty ε. Hence, it would be helpful to find a transform to simplify the circulant matrix and reduce the uncertainty. To simplify matrix $\mathbf{S}$, it is crucial to analyze ICI coefficient $\mathbf{S}(k,l)$ in (6) and the three parameters therein: k, l and ε. It is difficult to determine the relationship of these three parameters directly without first decomposing (6):

$$\begin{aligned} \mathbf{S}(k,l,\varepsilon) &= \frac{\sin[\pi(k-l+\varepsilon)]}{N\sin\left[\frac{\pi}{N}(k-l+\varepsilon)\right]} \\ &\cdot \exp\left[j\pi\left(1-\frac{1}{N}\right)(k-l+\varepsilon)\right] \\ &= \frac{1}{N}\cdot\frac{1-\cos[2\pi(k-l+\varepsilon)]-j\sin[2\pi(k-l+\varepsilon)]}{1-\cos\left[\frac{2\pi}{N}(k-l+\varepsilon)\right]-j\sin\left[\frac{2\pi}{N}(k-l+\varepsilon)\right]} \\ &= \frac{1}{N}\cdot\frac{1-\exp[j2\pi(k-l+\varepsilon)]}{1-\exp\left[j\frac{2\pi}{N}(k-l+\varepsilon)\right]} \\ &= \frac{1}{N}\sum_{l=0}^{N-1}\exp\left[j\frac{2\pi}{N}(k-l+\varepsilon)\right] \end{aligned}$$

$$\mathbf{S}(k,l,\varepsilon) = \frac{1}{N}\sum_{l=0}^{N-1}\exp\left(j\frac{2\pi}{N}k\right)\exp\left(j\frac{2\pi}{N}\varepsilon\right)\exp\left(-j\frac{2\pi}{N}l\right) . \quad (24)$$

It is now clear in (24) that $\mathbf{S}(k,l,\varepsilon)$ is a summation of exponential products with each exponent only being a function of a single parameter of interest. Using vector and matrix notation, $\mathbf{S}(k,l,\varepsilon)$ can be expressed as

$$\mathbf{S}(k,l,\varepsilon) = \frac{1}{\sqrt{N}}\,\mathbf{IDFT}(k,:)\cdot\mathbf{D}(\varepsilon)\cdot\frac{1}{\sqrt{N}}\,\mathbf{DFT}(:,l) , \quad (25)$$

where

$$\mathbf{IDFT}(k,:) = \left[e^{j\frac{2\pi}{N}k\cdot 0}, e^{j\frac{2\pi}{N}k\cdot 1}, \ldots, e^{j\frac{2\pi}{N}k\cdot(N-1)}\right]_{1\times N} ,$$

$$\mathbf{D}(\varepsilon) = \begin{bmatrix} e^{j\frac{2\pi}{N}\varepsilon\cdot 0} & & & \\ & e^{j\frac{2\pi}{N}\varepsilon\cdot 1} & & \\ & & \ddots & \\ & & & e^{j\frac{2\pi}{N}\varepsilon\cdot(N-1)} \end{bmatrix}_{N\times N} ,$$

$$\mathbf{DFT}(:,l) = \left[e^{-j\frac{2\pi}{N}l\cdot 0}, e^{-j\frac{2\pi}{N}l\cdot 1}, \ldots, e^{-j\frac{2\pi}{N}l\cdot(N-1)}\right]^T_{1\times N} .$$

The decomposition in (25) shows that the ICI coefficient $\mathbf{S}(k,l,\varepsilon)$ can be expressed as a product of the k^{th} row of normalized IDFT matrix $\mathbf{IDFT}(k,:)$, the $N \times N$ diagonal matrix $\mathbf{D}(\varepsilon)$, and the l^{th} column of normalized DFT matrix $\mathbf{DFT}(:,l)$. Therefore, the ICI coefficient matrix $\mathbf{S}$ can be written in the well-known eigen decomposition form as

$$\mathbf{S} = \mathbf{F}^H\mathbf{\Psi}\mathbf{F} , \quad (26)$$

where $\mathbf{F}$ is the normalized DFT matrix (the eigen matrix of $\mathbf{S}$ which is not a coincidence) and $\mathbf{\Psi}$ is the diagonal matrix $\mathbf{\Psi} = diag[\psi_0, \psi_1, ..., \psi_{N-1}]$ with diagonal elements (eigenvalues of matrix $\mathbf{S}$) given by $\psi_k = \exp\left(j\frac{2\pi\varepsilon k}{N}\right)$. It is important to note that $|\psi_k| = 1$ for all k. The received OFDM signal is now rewritten by substituting (26) into (19) and becomes

$$\vec{y} = \vec{x}\mathbf{F}^H\mathbf{\Psi}\mathbf{F} + \vec{n} , \quad (27)$$

with all the uncertainty now residing in diagonal matrix $\mathbf{\Psi}$.

B. Analysis of SC-OFDM Performance with ICI Present

Due to the perfect ICR performance of the SC-OFDM system, we next consider its performance with ICI present. Using the ICI coefficient matrix in (26) with $\mathbf{H} = \mathbf{I}$ for the AWGN channel, we revisit the expression in (16) and rewrite the received SC-OFDM signal vector as

$$\begin{aligned} \vec{y} &= \vec{y}\,\mathbf{F}\mathbf{S}\mathbf{F}^H + \vec{n}\,\mathbf{F}^H = \vec{x}\,\mathbf{F}\mathbf{F}^H\mathbf{\Psi}\mathbf{F}\mathbf{F}^H + \vec{n}\,\mathbf{F}^H \\ &= \vec{x}\,\mathbf{\Psi} + \vec{n}\,\mathbf{F}^H = \vec{x}\,\mathbf{\Psi} + \vec{n}\,' , \end{aligned} \quad (28)$$

where $\vec{n}\,' = \vec{n}\,\mathbf{F}^H$ has the same covariance matrix as $\vec{n}$ due to the orthonormality of the matrix $\mathbf{F}^H$. With the received signal on the k^{th} subcarrier corresponding to:

$$r_k = x_k\psi_k + n'_k . \quad (29)$$

Recalling that $|\psi_k| = 1$ for all k, it is noted that the ICI effect on SC-OFDM data symbols $\vec{x}$ is simply a (different) phase offset on each and every data symbol x_k. Compared with an OFDM system under similar ICI conditions, SC-OFDM provides significantly better performance. This is due to the received OFDM signal vectors in (27) being a combination of subcarrier data symbols and shifted responses thereof, while the subcarrier data symbols in the SC-OFDM signal vector

given by (28) only experience a phase offset–this is why we observe zero ICR for all ε and realize the benefit of SC-OFDM.

V. MKM For SC-OFDM Systems

After observing the ICI coefficient property, we find that $\mathbf{FSF}^H$ is a diagonal matrix with each diagonal element having unit magnitude. Hence, the ICI has no effect on the magnitude of each and every SC-OFDM data symbol. Therefore, when there is no noise present (29) shows that $|r_k| = |x_k|$ independent of ε. To fully exploit the inherent ICI immunity in SC-OFDM, we introduce a novel digital modulation scheme called Magnitude Keyed Modulation (MKM). Specifically, we will only use the magnitude to carry digital symbols. For example, binary MKM (2MKM) is equivalent to binary On-Off Keying (OOK). Note that MKM is different than Amplitude Shift Keying (ASK) using antipodal signal pairs given that MKM is a non-coherent modulation scheme and doesn't require phase reference.

According to (29), the decision of the k^{th} data symbol can be easily made for SC-OFDM using MKM:

$$\hat{x}_k = |r_k| \ . \tag{30}$$

A. BER Performance Analysis

For 2MKM, the BER performance is exactly the same as OOK with non-coherent detection given by

$$\begin{aligned} BER &= P(\hat{x}_k = 1|x_k = 0)P(x_k = 0) \\ &+ P(\hat{x}_k = 0|x_k = 1)P(x_k = 1) \\ &= \left[Q_1\left(0, \sqrt{SNR}\right) + 1 - Q_1\left(2\sqrt{SNR}, \sqrt{SNR}\right)\right]/2 \ , \end{aligned} \tag{31}$$

where Q_1 is the Marcum Q-Function [32] defined as

$$Q_M(\alpha, \beta) = \frac{1}{\alpha^{M-1}} \int_{\beta}^{\infty} x^M e^{-\left(x^2+\alpha^2\right)/2} I_{M-1}(\alpha x) dx \ , \tag{32}$$

where $I_n(x)$ is a modified Bessel function of the first kind [33]. It can also be written in series form as

$$Q_M(\alpha, \beta) = e^{-\left(\alpha^2+\beta^2\right)/2} \sum_{k=1-M}^{\infty} \left(\frac{\alpha}{\beta}\right)^k I_k(\alpha\beta) \ . \tag{33}$$

For L-MKM, the same process is used to derive the Symbol Error Ratio (SER) performance as:

$$\begin{aligned} SER &= \sum_{m=0}^{L-1} P(\hat{x}_k \neq m|x_k = m)P(x_k = m) \\ &= \sum_{m=0}^{L-1} P(\hat{x}_k \neq m|x_k = m)/L \\ &= Q_1(0, 0.5\lambda)/L \\ &+ \sum_{m=1}^{L-2} \left\{\left(1 - Q_1\left[m\lambda, (m-0.5)\lambda\right] + Q_1\left[m\lambda, (m+0.5)\lambda\right]\right\}/L \\ &+ \left\{1 - Q_1\left[(L-1)\lambda, (L-1-0.5)\lambda\right]\right\}/L \end{aligned} \tag{34}$$

where $\lambda = \frac{Signal\ Amplitude}{\sqrt{Noise\ Power}} = \sqrt{\frac{12 \cdot SNR \cdot \log_2(L)}{(L-1)(2L-1)}}$, and the resultant MKM BER can be approximated using the following assuming Gray Code symbol assignment [34] [35]:

$$BER \approx SER/\log_2(L) \ . \tag{35}$$

B. PAPR Performance Analysis

Since an important benefit of an SC-OFDM system is a much lower PAPR when compared with conventional OFDM, it is necessary to analyze the PAPR performance for SC-OFDM with MKM. This is done using one particular definition of discrete PAPR of an OFDM symbol: the maximum amplitude squared divided by the mean power of discrete symbols in the time domain [36].

Given time domain symbol vector $\vec{s} = [s_0, s_1, ..., s_{N-1}]$, with maximum amplitude of $||\ \vec{s}\ ||_\infty = max(|s_0|, |s_1|, ..., |s_{N-1}|)$ and mean power of $||\ \vec{s}\ ||_2^2 = (|s_0|^2 + |s_1|^2 + ... + |s_{N-1}^2|)/N$, the PAPR of $\vec{s}$ is

$$PAPR = \frac{||\ \vec{s}\ ||_\infty^2}{||\ \vec{s}\ ||_2^2} \ . \tag{36}$$

For an OFDM system with BPSK modulation, when the signal in time domain converges to one peak (e.g., in frequency domain $x_k = (-1)^k$), the worst PAPR is obtained and equals N. However, for single carrier systems such as SC-OFDM with MPSK (BPSK, QPSK, etc.) modulation, the maximum amplitude squared equals to the mean power in the time domain and therefore PAPR$= 1 \ll N$. Unlike SC-OFDM with MPSK modulation, the SC-OFDM system with MKM cannot retain the PAPR$= 1$ feature since the magnitude (amplitude) varies for different symbols in time domain. However, as shown next the SC-OFDM system with MKM has a much lower PAPR than an OFDM system with either PSK or MKM.

To compare the PAPR for different systems, we analyze the Cumulative Distribution Function (CDF) of the PAPR defined in (36) and given by

$$P(PAPR \leq z) = CDF(z) \ , \tag{37}$$

and provide simulated CDF plots of PAPR in Fig. 5, where PAPR of OFDM with QPSK is overlapped with PAPR of OFDM with 8PSK. These results are based on Monte Carlo simulation with 10^5 trials using $N = 256$ total subcarriers and configurations that included OFDM and SC-OFDM systems with various combinations of BPSK, 2MKM, QPSK, 4MKM, 8PSK, and 8MKM modulations as indicated. The minimum and maximum values in the plots, along with average PAPR, are presented in Table I. The metrics "Minimum", "Maximum" and "Average" in Table I indicate the smallest, largest and average observed PAPR in the simulation, respectively. In Fig. 5, the "Minimum" PAPR denotes the largest value for CDF is zero, the "Maximum" PAPR denotes the smallest value for the CDF is one.

The results in Table I clearly show that the SC-OFDM system consistently has the lowest PAPR, and that all combinations of SC-OFDM with MPSK modulation maintain a PAPR$= 0$ dB for all M. For combinations with higher modulation order ($M = 4$ and $M = 8$), i.e., SC-OFDM with MKM and OFDM with both MKM and PSK, PAPR is non-zero and the OFDM systems always produce a higher PAPR for any given modulation type and order. When comparing

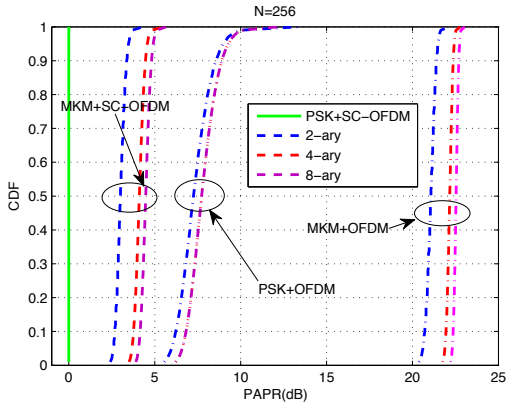

Fig. 5. CDF of PAPR for Different Modulation Orders

TABLE I
COMPARISON OF PAPR (DB) FOR DIFFERENT SYSTEM CONFIGURATIONS

Configuration	Maximum	Minimum	Average
OFDM+BPSK	13.76	4.38	7.34
OFDM+2MKM	22.15	19.78	21.06
SC-OFDM+BPSK	0	0	0
SC-OFDM+2MKM	4.59	2.01	3.02
OFDM+QPSK	12.54	5.29	7.81
OFDM+4MKM	22.80	21.27	22.16
SC-OFDM+QPSK	0	0	0
SC-OFDM+4MKM	5.42	3.07	4.11
OFDM+8PSK	12.24	5.29	7.81
OFDM+8MKM	23.03	21.92	22.53
SC-OFDM+8PSK	0	0	0
SC-OFDM+8MKM	5.70	3.45	4.48

results for a given modulation order, SC-OFDM with MKM always results in a lower PAPR relative to the corresponding OFDM system using either PSK or MKM.

C. Multipath Fading Channel

Now considering the case where multipath fading is present and matrix $\mathbf{H} \neq \mathbf{I}$, the ICI coefficient matrix in (26) is again substituted into (16) to form the received SC-OFDM signal vector as follows:

$$\vec{r} = \vec{x}\,\mathbf{FHSF}^H + \vec{n}\,\mathbf{F}^H = \vec{x}\,\mathbf{FH}\left[\mathbf{F}^H\mathbf{\Psi}\mathbf{F}\right]\mathbf{F}^H + \vec{n}\,\mathbf{F}^H = \vec{x}\,\mathbf{FHF}^H\mathbf{\Psi} + \vec{n}\,' \tag{38}$$

Similar to the procedure used for the AWGN channel, we can again use $|\vec{r}|$ to make decisions without the impact of the ε. Specifically, the decision of N data symbols $\hat{\vec{x}}$ can be determined by

$$\hat{\vec{x}} = arg\,\min_{\hat{\vec{x}}}(||\hat{\vec{x}}\mathbf{FHF}^H| - |\vec{r}||^2)\ , \tag{39}$$

which means $\hat{\vec{x}}$ is the symbol vector which can minimize the cost function $||\hat{\vec{x}}\mathbf{FHF}^H| - |\vec{r}||^2$. Since this procedure is similar to a multi user detection (MUD) and exhausted search algorithm is applied, the complexity is much higher compared the decision procedure in (30) for AWGN channel.

VI. SIMULATION RESULTS

The BER performance of the proposed SC-OFDM system with MKM modulation is first examined. Specifically, we compare performance of 1) SC-OFDM with binary MKM versus OFDM/SC-OFDM/MC-CDMA with BPSK modulation, 2) SC-OFDM with 4MKM versus OFDM/SC-OFDM/MC-CDMA with QPSK, and 3) SC-OFDM with 8MKM versus OFDM/SC-OFDM/MC-CDMA with 8PSK/8QAM, under conditions consistent with a high speed mobile environment. The stop criterion for simulations is the number of bit errors is larger than 1000.

The simplest way to examine the effectiveness of the proposed ICI immune SC-OFDM system using MKM modulation is to transmit signals through a AWGN channel using a constant transmitter-receiver NCFO (recall that NCFO $= \varepsilon = f_0/\Delta f$). The labeling convention for plotted BER results in the following figures is as follows: green line with circle markers–OFDM with PSK modulation; blue line with triangle markers–SC-OFDM with PSK modulation; purple line with diamond markers–MC-CDMA with PSK modulation; red rectangular–SC-OFDM system with proposed MKM modulation; cyan dot line–analytical performance for SC-OFDM system with proposed MKM modulation. Yellow line with stars–OFDM with 8QAM modulation; blue line with diamonds–SC-OFDM with 8 QAM modulation; black line with triangles–MC-CDMA with 8QAM modulation in Fig. 7(b). Performance of the baseline OFDM system using PSK modulation without ICI present is shown as the black line with dot markers, where theoretical BER performance is illustrated as baseline in Fig. 6 and Fig. 7 [35] [36], and simulation BER performance is illustrated as baseline in Fig. 9.

Fig. 6 shows simulated BER versus SNR for OFDM, SC-OFDM and MC-CDMA systems with binary modulation, $N = 64$ subcarriers, and AWGN channel conditions. These results were generated for normalized CFO of $\varepsilon = 0.3$. With high NCFO $\varepsilon = 0.3$, OFDM/SC-OFDM/MC-CDMA systems with BPSK modulation break down, and the proposed system outperforms these benchmarks significantly when SNR is high ($\geq 4dB$).

Fig. 7 shows simulated BER versus SNR for OFDM, SC-OFDM and MC-CDMA systems with 4MKM, QPSK, 8MKM, 8PSK and 8QAM modulations, $N = 64$ subcarriers, AWGN channel conditions, and NCFO values of $\varepsilon \in [0.1, 0.2]$. When compared with Fig. 6 results which show that the benefit of SC-OFDM with 2MKM is realized for $\varepsilon = 0.3$ at all SNR, results in Fig. 7(a) show that SC-OFDM with 4MKM outperforms other configurations when $\varepsilon = 0.2$ and SNR ≥ 6.0 dB (the other two systems are virtually unusable under these same conditions). A similar trend is observed in

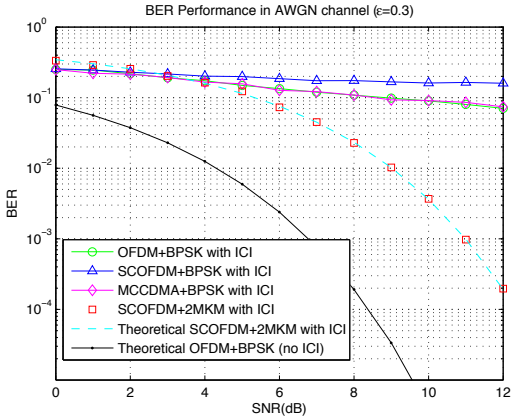

Fig. 6. AWGN Channel: BER vs. SNR for OFDM & SC-OFDM with binary modulations, $N = 64$ subcarriers, and $\varepsilon = 0.3$

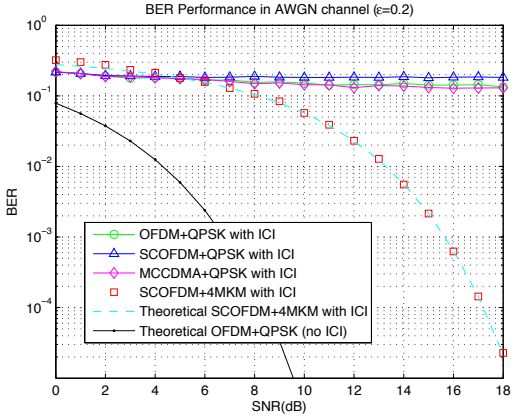

(a) Case 1: 4-ary Modulations with $\varepsilon = 0.2$

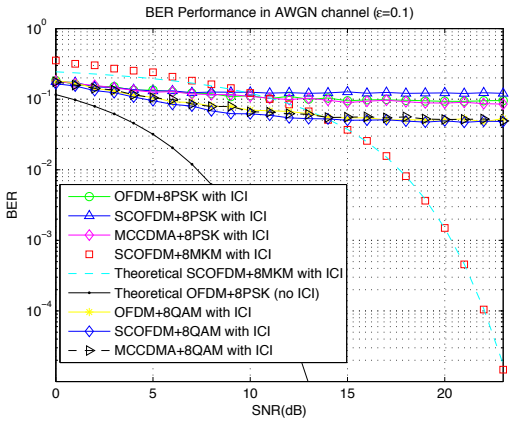

(b) Case 2: 8-ary Modulations with $\varepsilon = 0.1$

Fig. 7. AWGN Channel: BER vs. ε for OFDM & SC-OFDM using $N = 64$ subcarriers with indicated modulation order and ε values.

Fig. 7(b) results which show that SC-OFDM with 8MKM provides an advantage for $\varepsilon = 0.1$ and SNR ≥ 10.0 dB while the other systems are again unusable.

Final simulated AWGN results are presented in Fig. 8 which shows BER versus NCFO ε for OFDM/SC-OFDM/MC-CDMA using $N = 64$ subcarriers, SNR= 10dB, $\varepsilon \in [0.1, 1.1]$ (includes fractional and integer components), and binary, 4-

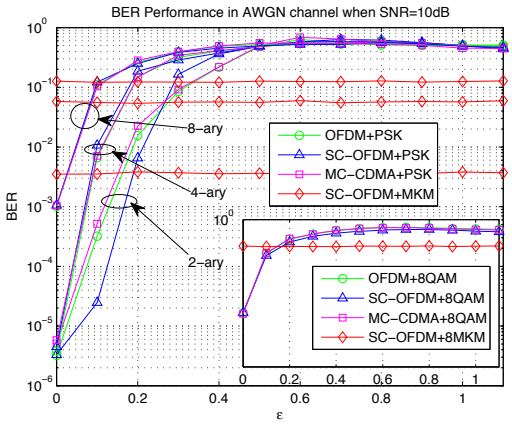

Fig. 8. AWGN Channel: BER vs. ε for OFDM & SC-OFDM using $N = 64$ subcarriers, $SNR = 10$ dB, and indicated modulation order.

ary, and 8-ary modulation orders. These results illustrate that the BER performance of SC-OFDM with 2MKM, 4MKM, and 8MKM remains constant as ε increases, while the BER performances of traditional OFDM/SC-OFDM/MC-CDMA systems with BPSK, QPSK, 8PSK and 8QAM modulations degrade significantly and catastrophically (approaches 0.5 in the worst cases).

By comparing Fig. 6 to Fig. 8 results, it is readily apparent that when ε increases or higher order modulation is used, the SC-OFDM system with the newly proposed MKM modulation significantly outperforms all OFDM/SC-OFDM/MC-CDMA systems using conventional PSK/QAM modulations. More specifically, SC-OFDM with MKM maintains nearly identical BER performance independent of ε variation while OFDM/SC-OFDM/MC-CDMA with PSK/QAM are very sensitive to changes, especially when using higher order modulations.

It is important to note that in these simulations we assumed that ε was a small fractional number, consistent with a residual CFO contribution that may remain after some types of cancellation or estimation processing have been applied in a PSK/QAM system. It is obvious from our results that OFDM/SC-OFDM/MC-CDMA systems using PSK/QAM are virtually useless when this residual ε exists. However, we have demonstrated that the SC-OFDM system with MKM modulation maintains nearly constant performance regardless of the fractional ε value and without requiring any additional processing. As a final note of validation, Fig. 6 and Fig. 7 provide theoretical BER performance for comparison with simulated results for proposed system (SC-OFDM with MKM). As evident in both figures, theoretical and simulated performances are equivalent which validates the analytic BER results for SC-OFDM with MKM, specifically, SC-OFDM with binary MKM in (31) and SC-OFDM with L-ary MKM in (35).

In a practical mobile multipath radio channel, time-variant multipath propagation leads to random Doppler frequency shift. For our final results we characterize performance of the proposed ICI cancellation method in a multipath fading channel. As a measure of Doppler frequency, we use the

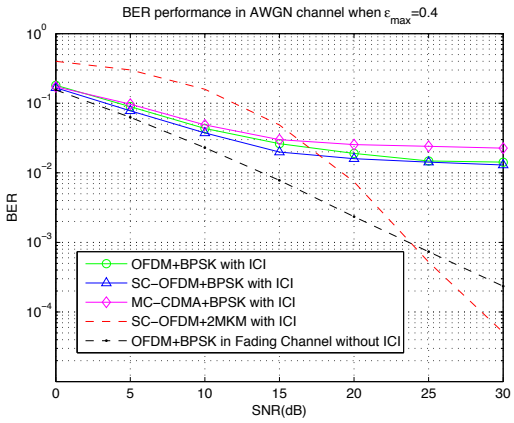

Fig. 9. Multipath Fading Channel: BER vs. SNR for OFDM & SC-OFDM with binary modulation, $N = 16$ subcarriers, and $\varepsilon_{max} = 0.4$.

normalized maximum Doppler spread ε_{max}, defined here as the ratio of channel maximum Doppler spread to subcarrier bandwidth. We assume a 4-fold multipath fading channel such that:

$$BW = N \cdot \Delta f = 4 \cdot \Delta f_c \tag{40}$$

where BW is the total system bandwidth and Δf_c is the channel coherence bandwidth.

Simulated BER performances for a multipath fading channel are provided in Fig. 9 for OFDM/SC-OFDM/MC-CDMA systems with binary modulation, $N = 16$ subcarriers, and $\varepsilon_{max} = 0.4$. The observations here are consistent with previous AWGN results: 1) SC-OFDM with the newly proposed 2MKM modulation is the most robust combination and virtually unaffected by ε_{max}, and 2) when SNR is high ($\geq 18dB$), performance for the OFDM/SC-OFDM/MC-CDMA systems with conventional BPSK modulation is poorer and a BER floor ($\approx 10^{-2}$) is observed.

VII. Conclusion

In this paper, we analyze the effect of ICI on an SC-OFDM receiver and propose a novel modulation scheme called Magnitude-Keyed Modulation (MKM) for use with an SC-OFDM system. Taking advantage of unique ICI coefficient matrix properties, we showed that the ICI effect on a received SC-OFDM signal is simply a phase offset on each and every data symbol, while the magnitude of the data symbol is unaffected. Hence, by transmitting digital information only on the SC-OFDM signal magnitude, the authors develop a novel modulation scheme called MKM and apply it to an SC-OFDM system. The resultant SC-OFDM system with MKM modulation experiences a boost in ICI immunity and significantly outperforms traditional OFDM, SC-OFDM and MC-CDMA systems using Phase Shift Keying (PSK) modulation and Quadrature amplitude modulation (QAM) in severe ICI environments. Simulation results are presented for SC-OFDM with binary, 4-ary, and 8-ary MKM modulations and the performance of each configuration compared with traditional OFDM/SC-OFDM/MC-CDMA using PSK/QAM modulation. Results for both AWGN and multipath fading channels clearly demonstrate that SC-OFDM with MKM is superior–much less BER degradation is observed as normalized carrier frequency offset and normalized Doppler spread increase.

References

[1] S. Hara and R. Prasad, *Multicarrier Techniques for 4G Mobile Communications*. Artech House, first ed., 2003.

[2] W. M. Jang, L. Nguyen, and P. Bidarkar, "MAI and ICI of synchronous downlink MC-CDMA with frequency offset," *IEEE Trans. Wireless Commun.*, vol. 5, pp. 693–703, Mar. 2006.

[3] T. R. Wang, J. G. Proakis, E. Masry, and J. R. Zeidler, "Performance degradation of OFDM systems due to Doppler spreading," *IEEE Trans. Wireless Commun.*, vol. 5, pp. 1422–1432, June 2006.

[4] Y. Zhao and S.-G. Haggman, "Intercarrier interference self-cancellation scheme for OFDM mobile communication systems," *IEEE Trans. Commun.*, vol. 49, pp. 1185–1191, July 2001.

[5] A. Seyedi and G. Saulnier, "General ICI self-cancellation scheme for OFDM systems," *IEEE Trans. Veh. Technol.*, vol. 54, pp. 198–210, Jan. 2005.

[6] H.-G. Ryu, Y. Li, and J.-S. Park, "An improved ICI reduction method in OFDM communication system," *IEEE Trans. Broadcasting*, vol. 51, pp. 395–400, Sept. 2005.

[7] Z. Jianhua, H. Rohling, and Z. Ping, "Analysis of ICI cancellation scheme in OFDM systems with phase noise," *IEEE Trans. Broadcasting*, vol. 50, pp. 97–106, June 2004.

[8] S.-M. Tseng, Y.-C. Kuo, and Y.-T. Hsu, "Turbo ICI cancellation and LDPC decoding for OFDM systems," in *Adv. Technol. Commun.*, pp. 405–408, Oct. 2008.

[9] R. Zhou, X. Li, V. Chakravarthy, B. Wang, and Z. Wu, "Inter-carrier interference self-cancellation in synchronous downlink MC-CDMA system," *IEEE International Conf. Wireless Commun. Mobile Comput.*, pp. 739–743, 2009.

[10] X. Li, R. Zhou, V. Chakravarthy, S. Hong, and Z. Wu, "Total intercarrier interference cancellation for OFDM mobile communication systems," *IEEE Consumer Commun. Netw. Conf.*, pp. 1–5, Jan. 2010.

[11] H. Minn, P. Tarasak, and V. Bhargava, "OFDM frequency offset estimation based on BLUE principle," *IEEE Veh. Technol. Conf.*, vol. 2, pp. 1230–1234, Sept. 2002.

[12] A. J. Coulson, "Maximum likelihood synchronization for OFDM using a pilot symbol: Analysis," *IEEE J. Sel. Areas Commun.*, vol. 19, pp. 2495–2503, Dec. 2001.

[13] M. Morelli and U. Mengali, "An improved frequency offset estimator for OFDM applications," *IEEE Commun. Lett.*, vol. 3, pp. 75–77, Mar. 1999.

[14] H. Kobayashi, T. Fukuhara, H. Yuan, and Y. Takeuchi, "Proposal of single carrier OFDM technique with adaptive modulation method," *IEEE Veh. Technol. Conf.*, vol. 3, pp. 1915–1919, Apr. 2003.

[15] A. Czylwik, "Comparison between adaptive OFDM and single carrier modulation with frequency domain equalization," *IEEE Veh. Technol. Conf.*, vol. 2, pp. 865–869, May 1997.

[16] J. Tubbax, B. Come, L. V. der Perre, L. Deneire, S. Donnay, and M. Engels, "OFDM versus single carrier with cyclic prefix: a system-based comparison," *IEEE Veh. Technol. Conf.*, vol. 2, pp. 1115–1119, Oct. 2001.

[17] D. Falconer, S. L. Ariyavisitakul, A. Benyamin-Seeyar, and B. Eidson, "Frequency domain equalization for single-carrier broadband wireless systems," *IEEE Commun. Mag.*, vol. 40, pp. 58–66, Apr. 2002.

[18] N. Benvenuto and S. Tomasin, "On the comparison between OFDM and single carrier modulation with a DFE using a frequency-domain feedforward filter," *IEEE Trans. Commun.*, vol. 50, pp. 947–955, June 2002.

[19] C. R. Nassar, B. Natarajan, Z. Wu, D. Wiegandt, S. Zekavat, and S. Shattil, *Multi-carrier Technologies for Wireless Communications*. Springer, Fall 2001.

[20] D. A. Wiegandt, Z. Wu, and C. R. Nassar, "High-throughput, high performance OFDM via pseudo-orthogonal carrier interferometry spreading codes," *IEEE Trans. Commun.*, vol. 51, pp. 1123–1134, July 2003.

[21] D. A. Wiegandt, Z. Wu, and C. R. Nassar, "High-performance carrier interferometry OFDM WLANs: RF testing," *IEEE International Conf. Commun.*, vol. 1, pp. 203–207, May 2003.

[22] A. Chandra, *Diversity Combining for Digital Signals in Wireless Fading Channels: Analysis and Simulation of Error Performance*. LAP LAMBERT Academic, May 2011.

[23] J. van de Beek, M. Sandell, and P. Borjesson, "ML estimation of time and frequency offset in OFDM systems," *IEEE Trans. Signal Process.*, vol. 45, pp. 1800–1805, July 1997.

[24] F. Yang, K. H. Li, and K. C. Teh, "A carrier frequency offset estimator with minimum output variance for OFDM systems," *IEEE Commun. Lett.*, vol. 8, pp. 677–679, Nov. 2004.
[25] A. J. Al-Dweik, "Robust non data-aided frequency offset estimation technique," *IEEE International Symp. Personal, Indoor Mobile Radio Commun.*, vol. 2, pp. 1365–1369, Sept. 2004.
[26] X. N. Zeng and A. Ghrayeb, "A blind carrier frequency offset estimation scheme for OFDM systems with constant modulus signaling," *IEEE Trans. Commun.*, vol. 56, pp. 1032–1037, July 2008.
[27] L. Wu, X.-D. Zhang, P.-S. Li, and Y.-T. Su, "A blind CFO estimator based on smoothing power spectrum for OFDM systems," *IEEE Trans. Commun.*, vol. 57, pp. 1924–1927, July 2009.
[28] T. Roman and V. Koivunen, "Subspace method for blind CFO estimation for OFDM systems with constant modulus constellations," *IEEE Veh. Technol. Conf.*, vol. 2, pp. 1253–1257, June 2005.
[29] Y. Yao and G. B. Giannakis, "Blind carrier frequency offset estimation in SISO, MIMO, and multiuser OFDM systems," *IEEE Trans. Commun.*, vol. 53, pp. 173–183, Jan. 2005.
[30] X. Li, E. Like, Z. Wu, and M. Temple, "Highly accurate blind carrier frequency offset estimator for mobile OFDM systems," *IEEE International Conf. Commun.*, pp. 1–5, 2010.
[31] P. Moose, "A technique for orthogonal frequency division multiplexing frequency offset correction," *IEEE Trans. Commun.*, vol. 42, pp. 2908–2914, Oct. 1994.
[32] D. A. Shnidman, "The calculation of the probability of detection and the generalized Marcum Q-function," *IEEE Trans. Inf. Theory*, vol. 35, pp. 389–400, Mar. 1989.
[33] G. Arfken, *Mathematical Methods for Physicists*. Academic Press, 6 ed., June 2005.
[34] M. Gardner, *Knotted Doughnuts and Other Mathematical Entertainments*. W.H. Freeman & Company, Oct. 1986.
[35] J. Proakis, *Digital Communications*. McGraw-Hill Science/Engineering/Math, 4 ed., Aug. 2000.
[36] A. Goldsmith, *Wireless Communications*. Cambridge University Press, Aug. 2005.

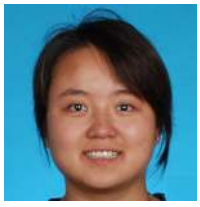

Xue Li (S'08) received the B.S. degree in electrical engineering from Tsinghua University, Beijing, China, in 2007 and the M.S. degree in electrical engineering from Wright State University, Dayton, OH, in 2008. She is currently pursuing the Ph.D. degree in the Department of Electrical Engineering, Wright State University.

Steven Hong (S'06) received his B.S. degree in Electrical Engineering from the University of Michigan, Ann Arbor in 2009, his M.S. degree in Electrical Engineering from Stanford University in 2011, and his Ph.D. in Electrical Engineering from Stanford University in 2012. His research interests include wireless networks, RF circuit design, and software systems.

Vasu D. Chakravarthy (M'98) is a Senior Electronics Engineer at Air Force Research Laboratories (AFRL), Sensors Directorate (SN), EW Techniques Development and Analysis Branch, and also serves as an adjunct faculty at Wright State University, Dayton OH. He received his B.S in Electrical Engineering from University of Illinois at Chicago in 1988, M.S and Ph.D. in Electrical Engineering from Wright State University in 1998 and 2008 respectively. Dr. Chakravarthy has been with AFRL since 1996 with an experience background in RF data links, Digital Receivers, Software GPS receivers and Communication Countermeasures. Research interest includes physical layer waveforms and signal processing algorithms related to Digital and Wireless Communications, issues related to Dynamic Spectrum Access, Cognitive Radio, Cognitive Jamming and Software Defined Radio technologies.

Michael A. Temple (SM'02) Professor of Electrical Engineering, Department of Electrical and Computer Engineering, (AFIT/ENG); BSE, Southern Illinois University, Edwardsville IL, 1985; MSE, Southern Illinois University, 1986; Ph.D., Air Force Institute of Technology, 1993. Dr. Temples research interests include passive emitter identification, tracking and location using RF Distinct Native Attribute (RF-DNA) fingerprinting and complex waveform generation using a Spectrally Modulated, Spectrally Encoded (SMSE) framework to improve digital communication efficiency. His sponsored research efforts in Command, Control, Communications and Intelligence (C3I) and Electronic Warfare (EW), as adopted by and/or transitioned to agencies within the US Department of Defense, has provided over $2M in R&D technology benefit. Dr. Temple has been a senior member of IEEE since January 2002.

Zhiqiang Wu (M'02) was born in Guiyang, China, in 1973. He received the B.S. degree from Beijing University of Posts and Telecommunications, Beijing, China, in 1993, the M.S. degree from Peking University, Beijing, in 1996, and the Ph.D. degree from Colorado State University, Fort Collins, in 2002, all in electrical engineering. Currently, he serves as an Associate Professor in the Department of Electrical Engineering, Wright State University, Dayton, OH.